J. Fluid Mech. (2009), *vol.* 641, *pp.* 245–261.
doi:10.1017/S0022112009991868

Electrically driven vortices in a weak dipolar magnetic field in a shallow electrolytic layer

ALDO FIGUEROA[1], FRANÇOIS DEMIAUX[2], SERGIO CUEVAS[1]† AND EDUARDO RAMOS[1]

[1]Centro de Investigación en Energía, Universidad Nacional Autónoma de México, A. P. 34, Temixco, Mor. 62580, México

[2]Mechanical Engineering Development Department, INSA-Lyon, 20 Av. Albert Einstein, 69621 Villeurbanne Cedex, France

(Received 29 September 2008; revised 31 August 2009; accepted 1 September 2009; first published online 25 November 2009)

Steady dipolar vortices continuously driven by electromagnetic forcing in a shallow layer of an electrolytic fluid are studied experimentally and theoretically. The driving Lorentz force is generated by the interaction of a dc uniform electric current injected in the thin layer and the non-uniform magnetic field produced by a small dipolar permanent magnet (0.33 T). Laminar velocity profiles in the neighbourhood of the zone affected by the magnetic field were obtained with particle image velocimetry in planes parallel and normal to the bottom wall. Flow planes at different depths of the layer were explored for injected currents ranging from 10 to 100 mA. Measurements of the boundary layer attached to the bottom wall reveal that owing to the variation of the field in the normal direction, a slightly flattened developing profile with no shear stresses at the free surface is formed. A quasi-two-dimensional magnetohydrodynamic numerical model that introduces the non-uniformity of the magnetic field, particularly its decay in the normal direction, was developed. Vertical diffusion produced by the bottom friction was modelled through a linear friction term. The model reproduces the main characteristic behaviour of the electromagnetically forced flow.

Key words: magnetohydrodynamic effects, MHD and electrohydrodynamics, vortex flows

1. Introduction

Electromagnetic forcing is a common experimental method to produce stirring in shallow layers of electrically conducting fluids. The idea is to produce a rotational Lorentz force by the injection of electric currents in a thin fluid layer exposed to a steady external magnetic field. This method has been widely used with the purpose of exploring the behaviour of quasi-two-dimensional flows which, incidentally, present similarities with those found in oceanic and atmospheric flows.

Past investigations on electromagnetically driven flows in shallow layers can be divided into two groups. In the first group the flow is enforced by injecting a steady electric current through a liquid metal layer under a strong uniform magnetic field normal to the layer (Sommeria 1986, 1988*a*, *b*; Messadek & Moreau 2002). Owing to the high electrical conductivity of liquid metals and the strong magnetic

† Email address for correspondence: scg@cie.unam.mx

field intensities, reached through electromagnets or superconducting magnets, the Hartmann number, which estimates the ratio of magnetic to viscous forces, can be very high. Under these conditions three-dimensional perturbations in the normal direction are suppressed by the action of the magnetic field (Sommeria 1986; Messadek & Moreau 2002). Sommeria & Moreau (1982) showed that flows between parallel insulating walls under a strong uniform magnetic field can be described in terms of a two-dimensional core flow with a linear friction (the Hartmann friction) that accounts for the effects of the boundary layers. This approach has been successfully applied to electromagnetically driven flows in shallow layers, where the two-dimensional Navier–Stokes equation includes both a steady forcing and a linear Hartmann friction term (Sommeria 1986, 1988*a*), and even inertial effects in Hartmann layers can be considered (Potherát, Sommeria & Moreau 2000).

The second group of electromagnetically driven shallow flows corresponds to those generated by the injection of electric currents in a thin layer of an electrolyte under a non-uniform magnetic field produced by an array of permanent magnets (Cardoso, Marteau & Tabeling 1994). The low electrical conductivity of electrolytes compared with that of liquid metals and the small magnetic field intensities produced by permanent magnets result in low-Hartmann-number flows. The geometrical confinement imposed by the shallow layer restricts three-dimensional perturbations in the normal direction. The use of two thin stably stratified fluid layers enhances the tendency of the flows towards two-dimensionality, since the density difference of the interface acts to prevent vertical velocities (Marteau, Cardoso & Tabeling 1995; Paret & Tabeling 1997). In shallow flows, the role of bottom friction is of fundamental importance, since it promotes a vertical diffusion, associated with the exponential damping of the flow. In purely hydrodynamic flows vertical diffusion is usually parameterized by adding a linear friction term (the Rayleigh friction) to the two-dimensional Navier–Stokes equation (Hansen, Marteau & Tabeling 1998; Clercx & van Heijst 2002; Clercx, van Heijst & Zoeteweij 2003). This approach can be applied for describing decaying vortex flows initially promoted by electromagnetic forces. Experimentally, relaxation regimes can be studied following the application of a short current impulse in the fluid layer (Cardoso *et al.* 1994; Marteau *et al.* 1995; Paret & Tabeling 1997; Paret *et al.* 1997; Hansen *et al.* 1998; Clercx *et al.* 2003). In this case, a purely hydrodynamic description is sufficient, since once the electric current is turned off, magnetohydrodynamic (MHD) effects can be disregarded because induced electric currents are usually negligible. However, for continuously electromagnetically forced shallow flows, MHD interactions cannot be disregarded, since the applied Lorentz force is always present. The understanding and modelling of these flows is important, since fundamental applications rely on a continuous stirring process. That is the case of mixing of a passive scalar with steady or periodic electromagnetic forcing (Williams, Marteau & Gollub 1997; Rothstein, Henry & Gollub 1999; Voth, Haller & Gollub 2002; Voth *et al.* 2003), the promotion of quasi-two-dimensional turbulence (Paret & Tabeling 1997; Tabeling 2002) or the generation of fully controllable multi-scale flows in laboratory (Rossi, Vassilicos and Hardalupas 2006*a*, *b*). However, to the best of our knowledge, a full MHD description of these phenomena has not been provided.

The objective of the present contribution is twofold. In the first place, the work is aimed at the experimental analysis of a dipolar vortex created in a thin layer of an electrolyte by the interaction of a steady, uniform electric current with the field produced by a single dipolar permanent magnet. This basic flow structure, usually present in a variety of scales in natural and laboratory flows, is also the building block of more complex flow patterns (e.g. Rossi *et al.* 2006*a*, *b*). By controlling the

intensity of the injected current in the shallow layer, we take advantage of the transparency of the electrolyte to explore the inner flow structure through particle image velocimetry (PIV) measurements in both planes parallel and normal to the bottom wall. Secondly, this paper also provides a quasi-two-dimensional model that contains the main physical ingredients of continuously electromagnetically forced laminar flows in shallow layers under localized magnetic fields. By taking only the dominant (normal) component of the non-uniform magnetic field within the shallow layer, which is fairly well reproduced analytically from the experimental distribution, the governing equations of motion are averaged in the normal direction. Since this average considers the decay of the field in the vertical direction, the model allows the calculation of the velocity field in planes at different depths in the layer. The comparison of the numerical and experimental velocity profiles shows a good quantitative agreement. The model appears to be particularly suited for the analysis of electromagnetically driven flows in shallow electrolytic layers.

2. Experimental procedure and observations

The experimental set-up consists of a rectangular frame of $28 \times 38 \times 1.6\,\mathrm{cm}$; one of the long sides and the two short sides are made of Plexiglas. The fourth side is made of glass. The frame is watertight glued to a thin floated glass plate 0.2 cm thick to form a cell with large horizontal area and small depth. Copper electrodes with rectangular cross-sections are placed along the shorter sides of the cell and connected to an adjustable dc voltage power supply. A permanent cylindrical neodynium–iron–boron dipole magnet with a diameter d of 1.9 cm and a height of 0.5 cm is placed under the glass plate with its upper flat face touching the lower side of the plate. The magnet is vertically magnetized with a maximum strength of 0.33 T at its surface. The cell is partially filled with a weak electrolytic solution of sodium bicarbonate ($NaHCO_3$) at 8.6 % by weight. The height, width and depth of the electrolyte layer are 0.4, 36 and 28 cm respectively, with a total volume of $400\,\mathrm{cm}^3$. The mass density, kinematic viscosity and electrical conductivity of the electrolyte are $\rho = 1.09 \times 10^3\,\mathrm{Kg\,m^{-3}}$, $\nu = 10^{-6}\,\mathrm{m^2\,s^{-1}}$ and $\sigma = 6.36\,\mathrm{S\,m^{-1}}$, respectively. The cell is mounted on a three-point support and levelled to get a horizontal layer of water solution with uniform thickness. The dc injected through the pair of electrodes interacts with the non-uniform magnetic field distribution, generating a rotational Lorentz force that sets the fluid in motion. In the experiments, electric currents varied within the range 10–100 mA. Owing to the distance from the electrodes to the observation region and the small magnitude of the electric currents, the electrochemical reactions occurring at the electrodes are negligible, as are the temperature changes because of Joule dissipation. Quantitative measurements of the velocity field were obtained with a PIV system (Dantec FlowMap PIV1100). We made two sets of flow measurements that required slightly different arrangements of the optical components of the system. In the first set, we observed the horizontal flow at different depths, while in the second, we observed the velocity field in a vertical plane perpendicular to the horizontal bottom wall (see figure 1).

2.1. *Flow measurements in horizontal planes*

In this observation, a laser sheet parallel to the bottom wall entered the cell through the vertical glass wall and illuminated an area of 4.6×28 cm. The x-coordinate and the y-coordinate lay on the horizontal plane, while the z-coordinate pointed in the normal direction. The origin was placed at the bottom wall at the point of maximum magnetic field strength. Flow images were captured with a Kodak model Megaplus ES1.0/Type

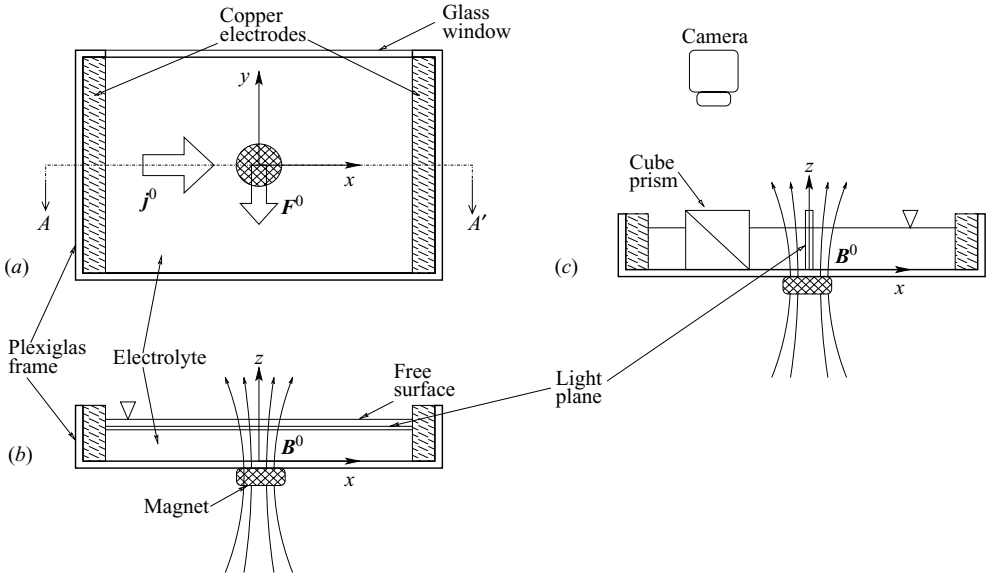

FIGURE 1. Sketch of the experimental device, not drawn to scale. (*a*) Plan view. (*b*) cross-sectional AA′ plane, showing the set-up for recording velocities in the horizontal plane. (*c*) cross-sectional AA′ plane, showing the set-up for recording velocities in the vertical plane. The imposed electrical current is denoted by $\boldsymbol{j}^0$ and the main direction of the Lorentz force by $\boldsymbol{F}^0$. Within the layer, the magnetic field $\boldsymbol{B}^0$ points mainly in the positive z-direction.

16 (30 Hz) camera, with a trigger synchronized with the illumination. The camera sat on a holder 20 cm above the fluid layer. The camera has a CCD of 1008×1016 pixels, and the actual area of the captured image is approximately 4.4×4.4 cm. The spatial deformation because of the proximity of the camera to the liquid layer was less than 1 mm in the x-direction and the y-direction and was compensated before making the analysis. Care was taken to ensure that the laser sheet and the bottom of the plate were parallel. To measure the thickness of the illuminating light, the laser sheet light was intercepted at the position of interest by a cubic 45° prism which deflected the beam in the vertical direction. The light was then captured at 0° of incidence by a camera, and the image was digitalized. Correcting for beam dispersion, a thickness of 0.07 ± 0.01 cm was determined. In the analysis, we used interrogation areas of 64×64 pixels with 50 % overlap in x and y and an adaptive correlation. These conditions gave us a spatial resolution of 0.13×0.13 cm. Preliminary experiments were used to find that maximum velocities were approximately 0.6 cm s^{-1} and 1.5 cm s^{-1} for electric currents of 25 mA and 100 mA, respectively. The time interval between two subsequent images for the majority of experiments was 50 ms. For the lowest measured velocities (corresponding to 10 mA), the time between images was 100 ms. Measurements of the flow in horizontal planes at different depths were obtained through lowering the stand of the laser by the required distance using fine pitch screws. The uncertainty in the vertical position of the recording plane was precisely the width of the laser sheet. Sample PIV measurements at selected points at different depths of the fluid layer were double-checked using laser Doppler anemometry (LDA) whose resolution in the vertical direction is approximately 1 mm. The readings with the two techniques agree to within the error of the LDA. Based on the maximum velocity near the free surface ($z = 3.5$ mm) and the diameter of the magnet, the Reynolds numbers of the

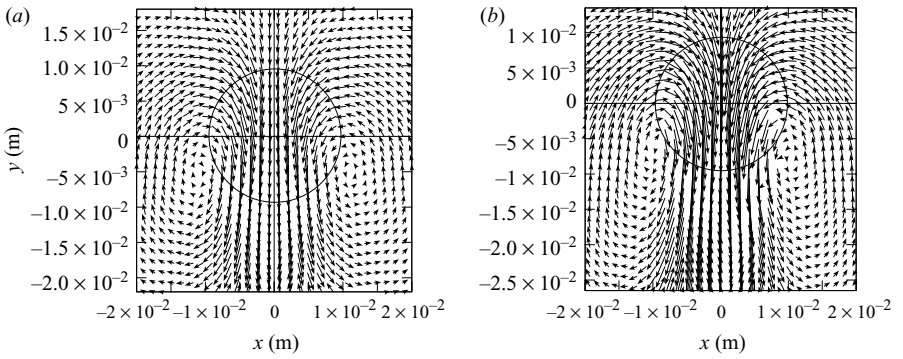

FIGURE 2. Velocity field for (*a*) $I = 25\,\text{mA}$ and (*b*) $I = 50\,\text{mA}$. For the velocity scale, see figures 7 and 8. The circle corresponds to the position of the magnet; $z = 3.5\,\text{mm}$, $B_{max} = 0.14$ T ($Ha = 0.20$).

flow varied from 50, for injected currents of 10 mA, to 290, for 100 mA. In turn, the Hartmann number $Ha = B_{max} h \sqrt{\sigma/\rho\nu}$ was based on the maximum magnetic field strength B_{max} at a height h from the bottom wall. Hence, Ha varied from 0.32 at the bottom to 0.19 at the free surface.

Owing to the experimental configuration, a quasi-two-dimensional flow structure was promoted where horizontal velocity components were much bigger than the vertical component (see § 2.2). Since the injected current and the dominant magnetic field component point in the positive x-direction and z-direction, respectively, the force points mainly in the negative y-direction. The flow develops a transient regime after which a well-defined steady flow pattern composed of two symmetric counter-rotating lobes (a vortex dipole) is reached. For small electric currents ($I \approx 10\,\text{mA}$) convective effects are small, and the flow is mainly governed by diffusion so that the vortex dipole displays symmetric patterns with respect to both x-axis and y-axis. Owing to the non-slip condition at the bottom wall, the highest velocities are located at the free surface of the electrolyte layer in a neighbourhood above the magnet along the y-axis. In this region the motion is similar to a plane jet with a broad base, with the fluid moving in the negative y-direction. The velocity field for a plane at a distance $z = 3.5\,\text{mm}$ from the bottom and an electric current $I = 25\,\text{mA}$ is shown in figure 2(*a*), where the circle indicates the position of the magnet. In the plane analysed, the magnitude of the maximum velocity is $5.8 \times 10^{-3}\,\text{m s}^{-1}$ ($Re = 110$) and is located at $x = 0$, $y = -4.5 \times 10^{-3}$ m. Figure 2(*b*) shows the velocity field when the electrical current is increased to 50 mA. Consequently, the maximum velocity is also increased reaching a magnitude of $9.8 \times 10^{-3}\,\text{m s}^{-1}$ ($Re = 186$) at $x = 0$, $y = -7.6 \times 10^{-3}$ m, further downstream from the point of maximum velocity for $I = 25\,\text{mA}$. The counter-rotating vortices are elongated in the direction of the force so that the centres of the recirculation structures (where the magnitude of the velocity is nearly zero) are displaced downstream. This is clearly a nonlinear convective effect that breaks the symmetry of the vortex dipole with respect to the x-axis. The general features of the velocity field are more clearly observed in figures 3(*a*)–3(*d*), where the velocity components u and v are plotted as functions of position for $I = 25\,\text{mA}$ at two different z-planes. Figures 3(*a*) and 3(*b*) correspond to $z = 3.5\,\text{mm}$, while figures 3(*c*) and 3(*d*) correspond to $z = 1.5\,\text{mm}$. Each figure contains both components, figures 3(*a*) and 3(*c*) as a function of the x-coordinate at $y = 0$ and figures 3(*b*) and 3(*d*) as a function of the y-coordinate at $x = 0$. Note that in general, the u velocity component is approximately an order of magnitude smaller than the v-component. The velocity distribution in

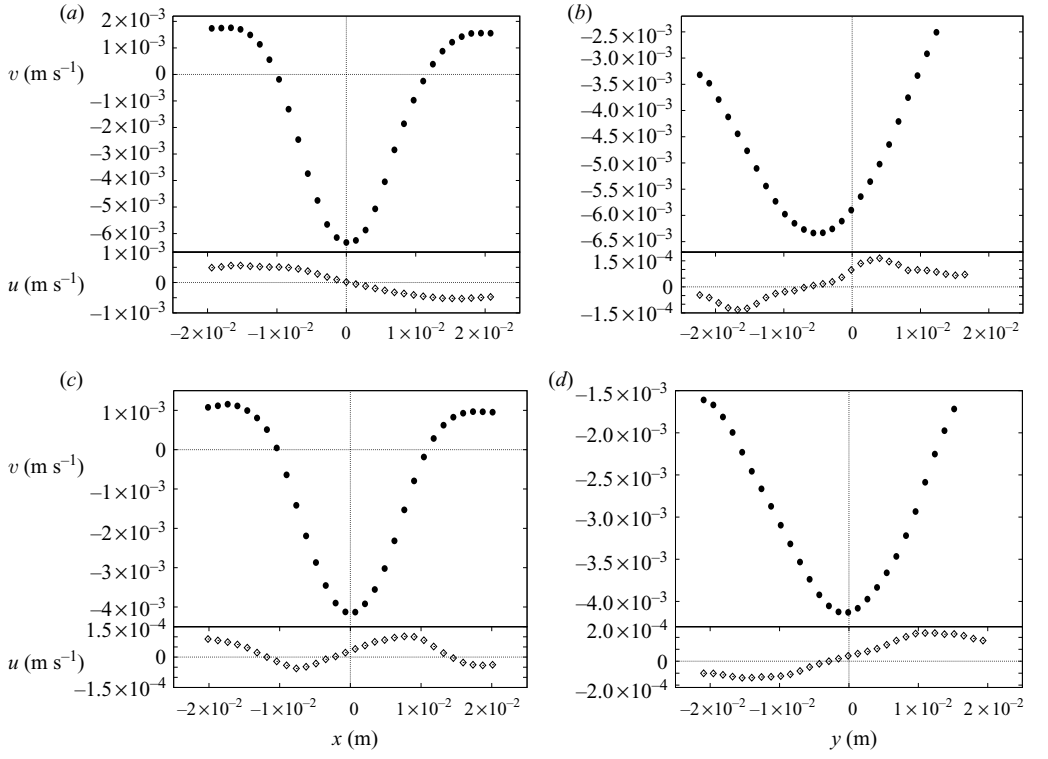

FIGURE 3. Velocities in the direction perpendicular (●) and parallel (◇) to the injected electric current as a function of position for $I = 25$ mA: (*a*) $y = 0$, $z = 3.5$ mm, $B_{max} = 0.14$ T ($Ha = 0.20$); (*b*) $x = 0$, $z = 3.5$ mm, $B_{max} = 0.14$ T ($Ha = 0.20$); (*c*) $y = 0$, $z = 1.5$ mm, $B_{max} = 0.19$ T ($Ha = 0.27$); (*d*) $x = 0$, $z = 1.5$ mm, $B_{max} = 0.19$ T ($Ha = 0.27$). Note the change of scale in the ordinates.

the direction perpendicular to the injected current (v-component, figures 3*a* and 3*c*) is nearly symmetric in the x-coordinate. The velocity profiles at the two z-planes are alike, the most salient difference being the attenuation of velocity at the plane closer to the bottom wall. In turn, the profile of the u-component (parallel to the injected current) as a function of the x-coordinate changes its shape from $z = 3.5$ mm to $z = 1.5$ mm as a result of a stronger bottom friction as well as a more intense Lorentz force. As a function of the y-coordinate, the v-component shows a marked asymmetry dictated by the main flow direction. This asymmetry is stronger at the plane $z = 3.5$ mm, closer to the free surface (see figure 3*b*), where convective effects displace the maximum velocity downstream from the point of maximum magnetic field strength. The influence of the bottom friction is clearly noticed in figure 3(*d*), where, in addition to the attenuation, the maximum v velocity is reached at the point of maximum magnetic field strength. To estimate the rate of attenuation as a function of the distance to the bottom wall, we made PIV measurements at planes normal to this wall.

2.2. *Flow measurements in vertical planes*

In order to get PIV measurements at planes normal to the bottom wall, we turned around the light sheet by 90° to obtain a vertical light plane which entered the cell through the glass wall. A 50/50 cubic prism ($2 \times 2 \times 2$ cm) was placed inside the

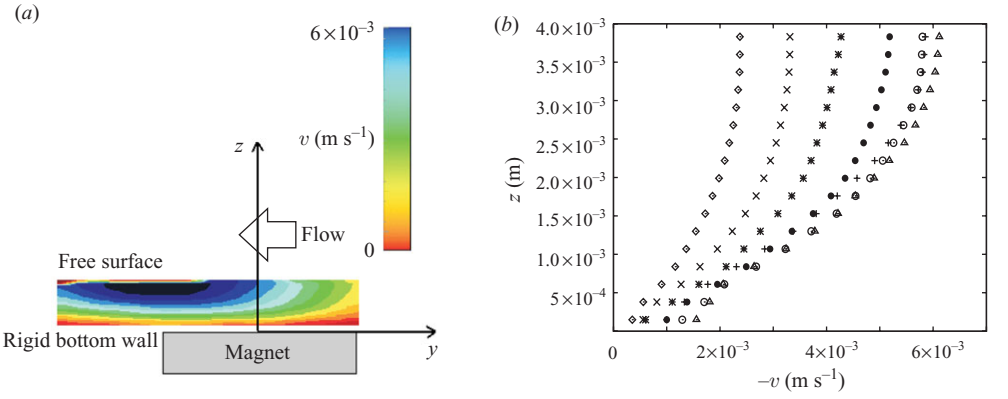

FIGURE 4. (*a*) Magnitude of the velocity component perpendicular to the injected electric current (v) at the vertical $x=0$ plane for $I=25$ mA. (*b*) Profiles of the v velocity component as a function of the depth z at the symmetry plane $x=0$, for different positions upstream and downstream of the magnet centre: ◇, $y=0.53d$; ×, $y=0.33d$; ∗, $y=0.19d$; ●, $y=0$; ⊙, $y=-0.19d$; △, $y=-0.38d$; +, $y=-0.58d$. At $z=0$, $B_{max}=0.22$ T ($Ha=0.32$).

cell at a distance of 15 cm from the illuminated plane. The light reflected by the particle tracers was refracted 90° by the prism and was captured by the camera, as shown in figure 1(*c*). The total area of analysis in this arrangement was 4.1×28 mm, and we used interrogation areas of 16×64 pixels or equivalently 0.23×0.92 mm. This relatively large-aspect-ratio interrogation area was used because the vertical velocity is extremely small. An adaptive correlation with an overlap of 50 % gave the best results. With this arrangement we could get a minimum of 18 points in the vertical direction, which is considered to resolve the boundary layer. In all reported PIV measurements, the rejected vectors were 2–3 %, which is smaller than the recommended 5 %. Observations in the plane normal to the bottom wall are useful to determine the quasi-two-dimensionality of the flow. The general feature of the flow as observed in the y–z plane is that the z-component of the velocity is undetectable with our experimental set-up, indicating that the flow is mostly in the horizontal direction with negligible vertical motion. In fact, no recirculations were observed in the y–z plane within the explored range of injected currents. Figure 4(*a*) displays the magnitude of the velocity as a function of the position in the vertical $x=0$ plane in the region above the magnet for $I=25$ mA. The figure shows the reduction of velocity as the fluid gets closer to the bottom wall, while because of convective effects, the overall maximum value is attained in the region close to the free surface, downstream from the point of maximum magnetic field strength. The flow development as the fluid traverses the non-homogeneous magnetic field region is shown in figure 4(*b*), where the negative of the y velocity component v as a function of the vertical coordinate z is displayed for several locations in the y-direction. All profiles are increasing functions of the coordinate z and display $\partial v/\partial z=0$ at the free surface. The maximum velocity at $y=0.53d$, the most upstream location observed, is a factor of three smaller than the corresponding value for $y=-0.58d$, which shows the acceleration transmitted to the fluid by the Lorentz force in this region. The global maximum velocity is observed downstream of the magnet centre at $y=-0.38d$, while at $y=-0.58d$, the flow has slowed down, and the velocity profile almost coincides with the profile at the position $y=-0.19d$. Mass is of course conserved, since at this location the flow is slightly divergent (see figure 2*a*). Owing to the presence of

the magnetic field, two distinctive features are displayed in these profiles, namely the flattening of the profiles, clearly observed at $y = 0.33d$, $y = 0.19d$ and $y = 0$, and the appearance of incipient inflection points close to the bottom wall. Since the Hartmann number is very small, the flattening cannot be attributed to induced effects but, as will be shown, to the variation of the applied field in the normal direction.

3. Theoretical model

The theoretical model considers the main features of the experimental situation, namely a thin layer of a conducting incompressible viscous fluid with a free surface, contained in a rectangular rigid box under a localized non-uniform magnetic field, $\boldsymbol{B}^0 = \boldsymbol{B}^0(x, y, z)$. The field is produced by a dipole magnet located at the insulating bottom wall with its dipole moment pointing in the normal z-direction, located at the geometrical centre of the container. A uniform steady electric current density injected in the positive x-direction interacts with the applied field, giving rise to a rotational Lorentz force that stirs the fluid. The total current density is given by the injected current plus the current induced by the motion of the fluid within the applied magnetic field. In turn, the total magnetic field is composed by the applied field plus the field generated by induced currents. We assume that the induced field remains very small in comparison with the applied field or, in other words, that the magnetic Reynolds number $Rm = \mu\sigma U_0 L$ is much less than unity, a condition fully satisfied in the experiment. Here, σ and μ are the electric conductivity and magnetic permeability of the fluid, respectively, and U_0 and L are a characteristic velocity and length, respectively, to be defined below. By neglecting $O(Rm)$ terms, the governing equations of motion can be expressed as

$$\nabla \cdot \boldsymbol{u} = 0, \tag{3.1}$$

$$\frac{\partial \boldsymbol{u}}{\partial t} + (\boldsymbol{u} \cdot \nabla)\boldsymbol{u} = -\frac{1}{\rho}\nabla p + \nu\nabla^2\boldsymbol{u} + \frac{1}{\rho}(\boldsymbol{j}^0 \times \boldsymbol{B}^0 + \boldsymbol{j}^i \times \boldsymbol{B}^0), \tag{3.2}$$

where the last term on the right-hand side of (3.2) considers the Lorentz force because of both the injected ($\boldsymbol{j}^0 = j^0\hat{\boldsymbol{x}}$) and induced ($\boldsymbol{j}^i$) current densities. In the same equation ρ and ν denote the mass density and kinematic viscosity of the fluid.

From the electromagnetic equations in the quasi-static approximation (Moreau 1990) we can get the so-called induction equation that, neglecting $O(Rm)$ terms, reads

$$0 = \frac{1}{\mu\sigma}\nabla^2\boldsymbol{b} + (\boldsymbol{B}^0 \cdot \nabla)\boldsymbol{u} - (\boldsymbol{u} \cdot \nabla)\boldsymbol{B}^0, \tag{3.3}$$

where the induced magnetic field $\boldsymbol{b}$ implicitly satisfies the equations

$$\nabla \cdot \boldsymbol{b} = 0, \tag{3.4a}$$

$$\nabla \times \boldsymbol{b} = \mu\boldsymbol{j}^i. \tag{3.4b}$$

Ampere's law (3.4b) gives an expression to calculate induced electric currents once $\boldsymbol{b}$ is determined and guarantees that the electric current density is divergence free, $\nabla \cdot \boldsymbol{j}^i = 0$. Further, the applied magnetic field $\boldsymbol{B}^0$ must satisfy the magnetostatic equations (Moreau 1990), which assure its solenoidal and irrotational character.

3.1. *Quasi-two-dimensional numerical model*

Vortical flows in shallow layers have been successfully modelled in both hydrodynamic (Zavala Sansón, van Heijst & Backx 2001; Clercx *et al.* 2003) and MHD flows (Sommeria 1988*a*), using a quasi-two-dimensional approach that involves the

integration (averaging) of governing equations in the vertical direction or along the magnetic field lines. Here, we follow an averaging approach recently presented by Cuevas, Smolentsev & Abdou (2006; see also Lavrent'ev *et al.* 1990; Smolentsev 1997) in the analysis of the flow past a localized magnetic field, where both Hartmann and classic viscous boundary layers are considered. However, in the present contribution an important difference is introduced, since the dependence of the applied magnetic field on the z-coordinate is considered.

A fundamental ingredient of the numerical solution is the accurate modelling of the applied magnetic field. In fact, for flows in shallow layers, a good agreement between numerical and experimental velocity fields depends to a great extent on a good theoretical reproduction of the dominant normal component according to the experimental measurements. The transversal components seem to have a weak influence. Therefore, we assume that the only non-negligible component is the normal one (straight magnetic field approximation; Alboussière 2004). For the permanent magnet used in the experiments, the normal dimensionless magnetic field component was reproduced analytically through the expression

$$B_z^0(X, Y, Z) = \mathscr{B}_z^0(X, Y)g(Z), \tag{3.5}$$

which is normalized by the maximum magnetic field strength at a given horizontal plane, B_{max}. Here, $\mathscr{B}_z^0(X, Y)$ reproduces the variation of the field in the $(X–Y)$ plane using an analytical expression for the field of a magnetized rectangular surface uniformly polarized in the normal direction (McCaig 1977). We considered the field created by the superposition of two parallel magnetized square surfaces of side length L, with opposing polarization axes and separated by a distance c, so that the external surfaces acted as the north and south poles of the permanent magnet; L was taken as the characteristic length in the $(X–Y)$ plane and was used to normalize the coordinates X and Y. Although experiments were carried out using a cylindrical magnet, a good fit with experimental values can be obtained using square magnetized surfaces provided measurements correspond to planes separated from the surface of the magnet, so that border effects are smoothed out. The strength of the normal component of the magnetic field was measured at different planes from the magnet surface corresponding with the flow planes experimentally explored using PIV. For each plane, the lengths L and c used in the fitting were chosen so that the distribution of magnetic field matched with the experimentally measured corresponding distribution. The comparison between experimental measurements and the fitting based on the expression by McCaig (1977) for the plane $z = 3.5$ mm is presented in figure 5(a). The fitting is excellent except in the neighbourhood of one of the edges of the magnet, where a small asymmetry in the field distribution is detected. Apart from this detail, the field distribution can be considered axially symmetric. In turn, the function $g(Z)$ in (3.5), which introduces the field variation in the normal direction, was obtained from the fitting of the experimental data in the form

$$g(Z) = \exp(-\gamma \varepsilon Z), \tag{3.6}$$

where Z is normalized by the depth of the layer h, at a given vertical position, and $\gamma = 2.05$. Here $\varepsilon = h/L$ is the aspect ratio that compares the characteristic lengths in the normal and transversal directions. Figure 5(b) compares the experimental measurements and the fitting obtained from (3.6).

In addition, we assume that the transport of momentum in the normal direction is mainly diffusive, so that the dimensionless velocity components in the $(X–Y)$ plane

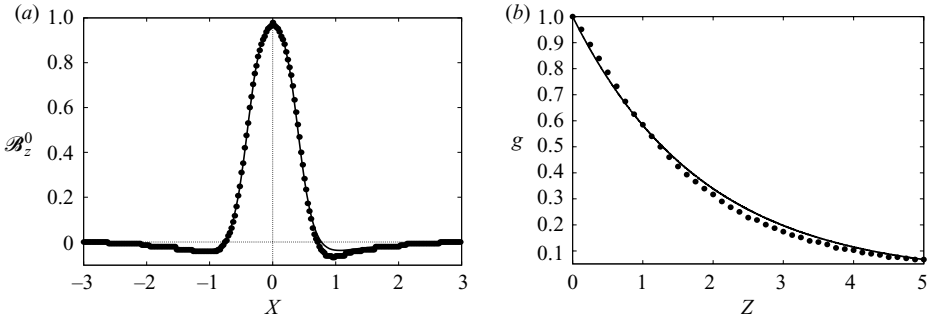

FIGURE 5. (*a*) Normalized z-component of the magnetic field at $z = 3.5\,\mathrm{mm}$ as a function of X. The continuous line is the fitting based on the analytic expression (see McCaig 1977) for magnetized surfaces of side length $L = 15.2\,\mathrm{mm}$ separated by a distance $c = 14\,\mathrm{mm}$. (*b*) Normalized z-component of the magnetic field as a function of the vertical coordinate Z. The region $Z \leqslant 1$ corresponds to the layer thickness. The continuous line is the fitting based on (3.6) with $\gamma = 2.05$. In both figures, black dots correspond to experimental measurements.

can be expressed as

$$U(X, Y, Z, T) = \bar{U}(X, Y, T)\ \hat{f}, \quad V(X, Y, Z, T) = \bar{V}(X, Y, T)\ \hat{f}. \tag{3.7}$$

The components U and V are normalized by $u_0 = \nu/L$, and time T is normalized by the viscous time L^2/ν. The functions $\bar{U}$ and $\bar{V}$ denote the averaged velocity components in the $(X$–$Y)$ plane. The function $\hat{f}$ may, in principle, depend on X, Y and Z and satisfies the normalization condition $\int_0^{\varepsilon} \hat{f}\,\mathrm{d}Z = 1$. According to the shallow-flow approximation, ε is assumed to be less than unity. (In the experiment, the maximum value of ε, obtained at the free surface, is 0.26.) The function $\hat{f}$ should reproduce the velocity profile in the normal direction both in the neighbourhood of the magnet and far from it. The explicit form of $\hat{f}$ can be obtained from a balance between viscous and Lorentz forces generated by both injected and induced currents. Since the applied Lorentz force points in the negative y-direction and is maximum in the centre of the magnet, we establish the balance at the central $(Y$–$Z)$ plane $(X = 0)$. Then, f must satisfy the equation

$$\frac{\mathrm{d}^2 f}{\mathrm{d}Z^2} - \left(Ha\mathscr{B}_z^0 g\right)^2 f = \varepsilon^2\, Re_*\, \mathscr{B}_z^0 g. \tag{3.8}$$

In (3.8) the function f has still to be normalized. In turn, the Reynolds number $Re_* = U_0 L/\nu$ is based on the characteristic bulk velocity $U_0 = j^0 B_{max} L^2/\rho\nu$, obtained from a balance between viscous and applied Lorentz forces. Note, however, that this balance only considers lateral viscous diffusion and does not take into account the friction at the bottom wall. Therefore, Re_* does not coincide with the experimental Reynolds number based on the maximum velocity at a given flow plane. The terms on the left-hand side of (3.8) correspond to the viscous and induced Lorentz forces, while the term on the right-hand side is the applied Lorentz force. Since in the experiments the Hartmann number is of order 10^{-1}, the induced Lorentz force in (3.8) can be neglected. Further, f must satisfy non-slip conditions at the bottom wall ($f(Z = 0) = 0$) and the absence of shear stresses at the free surface ($\mathrm{d}f/\mathrm{d}Z(Z = \varepsilon) = 0$). Once it is

normalized, $\hat{f}$ takes the form

$$\hat{f} = \frac{\left[\mathrm{e}^{-\gamma Z} + Z\gamma\varepsilon\,\mathrm{e}^{-\gamma\varepsilon^2} - 1\right]}{\frac{1}{\gamma\varepsilon}(1-\mathrm{e}^{-\gamma\varepsilon^2}) + \frac{\gamma\varepsilon^3}{2}\,\mathrm{e}^{-\gamma\varepsilon^2} - \varepsilon}. \tag{3.9}$$

Owing to normalization, $\hat{f}$ is independent of $\mathscr{B}_z^0$ and Re_*. An averaged quasi-two-dimensional system of equations can now be obtained if (3.5)–(3.7) and (3.9) are substituted in (3.1) and (3.2) and integrated in the Z-coordinate from 0 to ε, assuming that the bottom wall and the free surface are electrically insulated. If the electric current density and the induced magnetic field are normalized, respectively, by j^0 and RmB_{max}, it can be shown that the induced Lorentz force is of order Ha^2 and, consequently, can be neglected in (3.2). Therefore, the induction equation (3.3) is not relevant for the description, and the averaged equations of motion in dimensionless form read

$$\frac{\partial U}{\partial X} + \frac{\partial V}{\partial Y} = 0, \tag{3.10}$$

$$\frac{\partial U}{\partial T} + \left(U\frac{\partial U}{\partial X} + V\frac{\partial U}{\partial Y}\right) = -\frac{\partial P}{\partial X} + \nabla_\perp^2 U + \frac{U}{\tau}, \tag{3.11}$$

$$\frac{\partial V}{\partial T} + \left(U\frac{\partial V}{\partial X} + V\frac{\partial V}{\partial Y}\right) = -\frac{\partial P}{\partial Y} + \nabla_\perp^2 V + \frac{V}{\tau} - \alpha Re_*\mathscr{B}_z^0, \tag{3.12}$$

where the overline in the velocity components has been dropped; the pressure P is normalized by ρu_0^2; and the subindex $\perp$ denotes the projection of the ∇^2 operator on the $(X$–$Y)$ plane. Velocity components satisfy non-slip conditions at the boundaries of the container. Note that in the absence of injected current, $Re_* = 0$ and no motion exists. On the right-hand sides of (3.11) and (3.12) appears a linear friction term accounting for the effects of viscous boundary layer at the bottom wall. This term involves a (dimensionless) characteristic time scale τ, for the damping of vorticity owing to dissipation in the viscous layers, whose inverse is given by

$$\tau^{-1} = \frac{1}{\varepsilon^2}\frac{\mathrm{d}\hat{f}}{\mathrm{d}Z}\bigg]_0^\varepsilon = \frac{\gamma\left(1-\mathrm{e}^{-\gamma\varepsilon^2}\right)}{\frac{1}{\gamma}\left(1-\mathrm{e}^{-\gamma\varepsilon^2}\right) + \frac{\gamma\varepsilon^4}{2}\mathrm{e}^{-\gamma\varepsilon^2} - \varepsilon^2}. \tag{3.13}$$

Further, owing to the variation of the magnetic field in the normal direction, the Lorentz force term in (3.12) includes the factor α given by

$$\alpha = \int_0^\varepsilon g(Z)\,\mathrm{d}Z = \frac{1}{\gamma\varepsilon}\left(1-\mathrm{e}^{-\gamma\varepsilon^2}\right). \tag{3.14}$$

The inductionless system of equations (3.10)–(3.14) was used to model the electromagnetically driven flow at different depths in the shallow layer.

4. Comparison of numerical model with experimental observations

4.1. *The friction model*

In shallow flows, a good quantitative numerical reproduction of experimental results relies to a great extent on the correct assessment of bottom friction effects that, owing to the small value of the Hartmann number, in the present experiments are purely of viscous origin. In our simulation this is accomplished through the linear friction model (see (3.9)–(3.13)) that results from the averaging of the governing equations in the

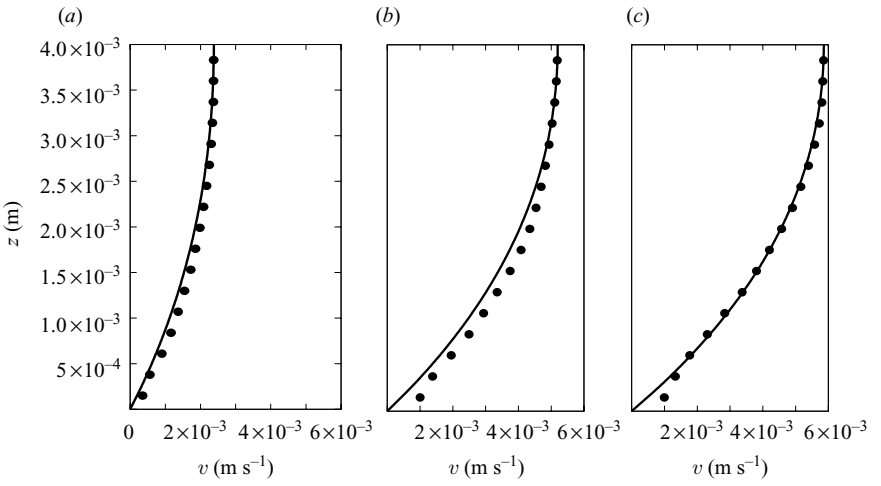

FIGURE 6. The v-component of velocity as a function of z for $I = 25$ mA at $x = 0$: (a) $y = 0.53\,d$; (b) $y = 0$; (c) $y = -0.58d$. The dots are experimental data, and the continuous lines show the scaled velocity profiles from (3.9).

normal direction, using the velocity distribution (3.9) in this direction. Reliability of the averaging procedure depends, in turn, on the proper modelling of the velocity profiles in the depth of the shallow layer. In figures 6(a)–6(c), the scaled analytical profiles given by (3.9) are compared with experimental profiles of the velocity component in the y-direction (v) as functions of the z-coordinate at different y-positions and at $x = 0$, corresponding to $I = 25$ mA. The continuous line in figure 6 shows the fit of the analytical velocity profile (3.9), properly scaled by a constant, obtained with the maximum aspect ratio, $\varepsilon = 0.26$. The comparison shown in figures 6(a)–6(c) indicates that the shape of the developing experimental profiles as the flow traverses the non-homogeneous magnetic field region can be adequately reproduced by the velocity profile (3.9) that considers the decay of the magnetic field strength in the vertical direction. In fact, the observed flattening of the profile seems to be due to this effect. It is therefore expected to be a reasonable assessment of the bottom friction based on this velocity profile. However, an important point has to be noted. A careful observation of experimental velocity profiles (see also figure 4b) reveals the existence of incipient inflection points located very close to the bottom wall that cannot be captured with profile (3.9).

4.2. *General features of the flow structure*

The system of equations (3.10)–(3.12) with the friction model based on (3.9) and (3.13) and the magnetic field distribution given from the analytic expression by McCaig (1977) was solved numerically in a rectangular domain corresponding to the dimensions of the experimental set-up, using a finite-difference method based on the procedure described in Griebel, Dornseifer & Neunhoeffer (1998), adapted to consider MHD flows. A detailed explanation of the numerical procedure can be found in Cuevas *et al.* (2006).

In figure 7, the velocity components in the horizontal plane predicted by the theoretical model (see § 3) are compared with experimental results for the case $I =$ 25 mA at the plane $z = 3.5$ mm ($Re_{max} = 110$). The symbols correspond to experimental values, while the continuous and dotted lines denote numerical predictions. Figure 7(a) shows both velocity components as functions of the x-coordinate at the centreline

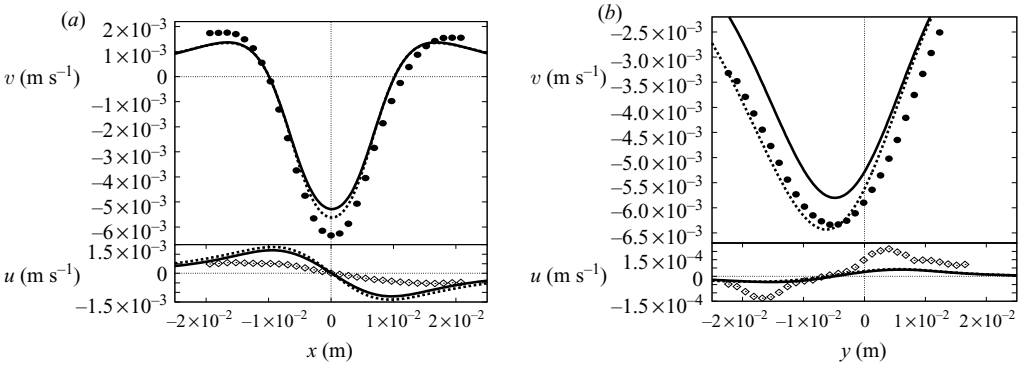

FIGURE 7. Experimental velocities in the direction perpendicular (●) and parallel (◇) to the injected electric current as functions of position for $I = 25\,\text{mA}$, $z = 3.5\,\text{mm}$: (*a*) $y = 0$, (*b*) $x = 0$. The continuous lines show numerical simulations for $I = 25\,\text{mA}$, $z = 3.5\,\text{mm}$. The dotted lines show numerical simulations for $I = 25\,\text{mA}$, $z = 4.0\,\text{mm}$.

$y = 0$. The velocity distribution is symmetric for the component v, in the direction perpendicular to the injected current, and antisymmetric for the component u, parallel to the injected current. The slight asymmetry of the experimental (positive) values of v reflects the corresponding asymmetry in the magnetic field distribution of the magnet shown in figure 5(*a*). The velocity profiles along the symmetry line ($x = 0$) are given in figure 7(*b*). As noted in § 2.1, owing to convective effects the maximum value of component v is not reached at $y = 0$ but downstream. The continuous lines correspond to numerical results obtained with the experimental conditions, $I = 25\,\text{mA}$, $B_{max} = 0.14\,\text{T}$ and $z = 3.5\,\text{mm}$ ($\varepsilon = 0.23$). The numerical prediction of the v profile as a function of x and y underestimates the magnitude of the velocity by less than 15 %; hence, a quasi-two-dimensional description of electromagnetically forced shallow laminar flows seems to be compatible with experimental results. In fact, the model reproduces the main physical effects observed experimentally. For instance, it predicts correctly the position at which the profile changes from negative to positive values (see figure 7*a*). Further, we observe in figure 7(*b*) that the position of the maximum velocity is correctly predicted, which indicates that convective effects are suitably captured by the model. The dotted lines in figure 7, which approach closer to the experimental results, correspond to the calculations performed for the plane $z = 4.0\,\text{mm}$ ($\varepsilon = 0.26$). Note that the difference in the plane position is within the uncertainty of the position of the laser sheet, namely $\pm 0.7\,\text{mm}$.

4.3. *Flow features as functions of the applied current*

The main effects of increasing the applied current is the elongation of the vortices in the main direction of the localized Lorentz force. This was briefly described in § 2.1 and is illustrated in figure 2(*b*). In fact, the centres of the recirculation regions as well as the location of maximum velocity are convected a larger distance in the direction of the main Lorentz force for larger electric currents. This effect is correctly predicted by the model. In table 1, the experimental y-positions of the maximum velocity as functions of the electrical current are shown together with the predictions of the model at the plane $z = 3.5\,\text{mm}$. In all cases, the abscissa of the maximum velocity is $x = 0$. The relative error is smaller than 18 % and less than 10 % for most cases.

In figure 8, the experimental results and numerical predictions of the absolute value of the maximum flow velocity (v_{max}) at the plane $z = 3.5\,\text{mm}$ are shown as

I (mA)	y_e (m)	y_n (m)	$(y_e - y_n)/\overline{y}$
10	-2.1×10^{-3}	-2.3×10^{-3}	−0.090
15	-3.5×10^{-3}	-3.3×10^{-3}	0.059
20	-4.9×10^{-3}	-4.1×10^{-3}	0.178
25	-4.5×10^{-3}	-4.9×10^{-3}	−0.085
30	-4.9×10^{-3}	-5.6×10^{-3}	−0.133
40	-6.2×10^{-3}	-6.6×10^{-3}	−0.062
50	-7.6×10^{-3}	-7.4×10^{-3}	0.026
60	-7.6×10^{-3}	-7.9×10^{-3}	−0.039
70	-9.0×10^{-3}	-8.4×10^{-3}	0.069
80	-9.0×10^{-3}	-8.6×10^{-3}	0.045
90	-1.04×10^{-2}	-8.9×10^{-3}	0.155
100	-1.04×10^{-2}	-9.1×10^{-3}	0.133

TABLE 1. The experimental y-positions of the points of maximum velocity as functions of electric current at $z = 3.5$ mm. The subscripts e and n indicate the experimental measurements and numerical calculations, respectively; $\overline{y} = (y_e + y_n)/2$.

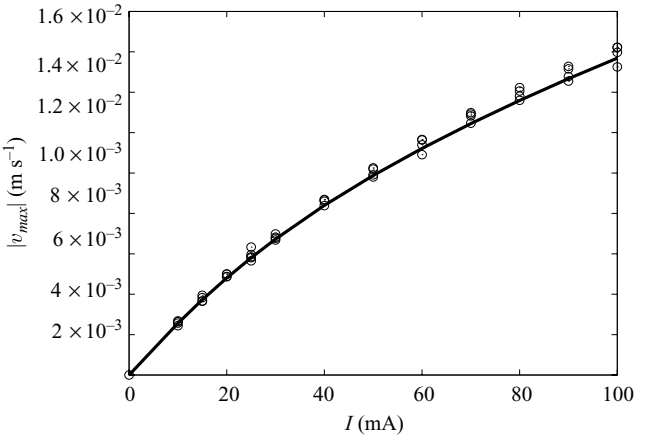

FIGURE 8. Absolute value of the maximum velocity ($|v_{max}|$) as a function of the applied current I at the plane $z = 3.5$ mm. Each symbol corresponds to an individual experimental observation. The continuous line corresponds to numerical simulations.

a function of the imposed electric current. Four measured values are reported in the curve for every electric current strength. The experimental observations fit the curve $|v_{max}| = -8 \times 10^{-7} I^2 + 2 \times 10^{-4} I + 5 \times 10^{-4}$. The numerical results present a very good quantitative agreement with experimental measurements in the full range of explored electric currents. These results indicate that the quasi-two-dimensional model is able to reproduce the steady electromagnetically forced flow in the shallow layer.

5. Concluding remarks

In the present contribution, we have described PIV observations of laminar vortex dipoles driven by the interaction of a uniform dc injected current and the field produced by a small permanent magnet in a shallow layer of an electrolyte. In contrast with high-Hartmann-number electrolytic flows (Andreev, Heberstroh & Thess 2001),

the very small values of Ha in the present experiment ($O(10^{-1})$) lead to negligible induced effects and to the predominance of viscous and imposed non-uniform Lorentz forces. Although several experimental studies have addressed the decay properties of vortical shallow flows of electrolytes initially generated by electromagnetic forcing, the detailed exploration and modelling of flows in shallow layers continuously stirred by localized electromagnetic forces have, to the best of our knowledge, not been previously considered. The presumption of quasi-two-dimensionality of these flows was corroborated by exploring flow planes parallel to the bottom wall at different depths as well as flow planes normal to this wall, so that an approximate three-dimensional picture of the flow structure was reconstructed. For small injected currents, a quite symmetric dipolar vortex structure is formed mainly by diffusive momentum transport. As the current is increased, convective effects are manifested by the elongation of the vortices in the main direction of the Lorentz force along with the displacement of the point of maximum velocity downstream. The damping of velocity owing to bottom friction was measured at flow planes close to the bottom wall and by looking at planes normal to that wall. In fact, it appears that the experimental measurement of velocity profiles in the vertical direction in electromagnetically driven shallow flows have been overlooked in the past. In spite of the weakness of the applied magnetic field, this information reveals developing velocity profiles with a shape that depends on the location within the non-uniform magnetic field region and, in particular, on the field strength in the normal direction. Based on the maximum velocity near the free surface, the Reynolds numbers of the flow varied from 50, for injected currents of 10 mA, to 290, for 100 mA. Under the explored conditions, no recirculations were observed in planes normal to the bottom wall, indicating that the transport of momentum in the normal direction is mainly diffusive. However, the velocity profiles at the entrance to the magnetic field region are marked by the appearance of incipient inflection points that, for stronger injected currents, might lead to the instability of the boundary layer. The exploration of this effect may deserve further study.

A quasi-two-dimensional model was introduced, and numerical simulations were compared with available experimental results. This simple model, which correctly captures the main physical features of the basic flow and avoids difficulties of a full three-dimensional approach, includes convective effects and involves the integration (averaging) of governing equations in the vertical direction. Since the depth of the electrolyte layer is much smaller than its horizontal extension, the local magnetic field originated by a permanent dipole magnet can be realistically approximated by considering only its component in the vertical direction. This assumption, which greatly simplifies the analysis, seems to be more justified for shallow flows than for duct flows in non-homogeneous magnetic fields (Alboussière 2004). The vertical field component is modelled analytically and fitted accurately to reproduce the experimental field. The results reported in the present study show that a quasi-two-dimensional flow description is suitable. In general, a good quantitative comparison is found between numerical results and experimental observations. One of the key elements that allows an accurate estimation of the bottom viscous friction and the magnitude of the Lorentz force is the consideration of the variation of the magnetic field strength in the vertical direction. In fact, the observed flattened profiles in the zone of more intense magnetic field are due precisely to this effect. The influence of inflection points on the global behaviour of the flow appears to be small and, as confirmed by the results presented in § 4, does not invalidate the quasi-two-dimensional description. The model is a useful tool for the analysis of steady electromagnetically

forced flows at low Hartmann and intermediate Reynolds (< 300) numbers in shallow layers of electrolytes.

The authors acknowledge insightful comments from an anonymous reviewer that helped to improve the comparison between theory and experiment. This research was supported by DGAPA-UNAM and CONACYT, Mexico, under projects IN103100 and 59977, respectively. A. Figueroa thanks a grant from CONACYT. Valuable comments of Sergey Smolentsev from the UCLA are thankfully acknowledged.

REFERENCES

Alboussière, T. 2004 A geostrophic-like model for large Hartmann number flows. *J. Fluid Mech.* **521**, 125–154.

Andreev, O., Heberstroh, Ch. & Thess, A. 2001 MHD flow in electrolytes at high Hartmann numbers. *Magnetohydrodynamics*, **37** (1–2), 151–160.

Cardoso, O., Marteau, D. & Tabeling, P. 1994 Quantitative experimental study of the free decay of quasi-two-dimensional turbulence. *Phys. Rev.* E **49** (1), 454–461.

Clercx, H. J. H. & van Heijst, G. J. F. 2002 Dissipation of kinetic energy in two-dimensional bounded flows. *Phys. Rev.* E **65**, 066305.

Clercx, H. J. H., van Heijst, G. J. F. & Zoeteweij 2003 Quasi-two-dimensional turbulence in shallow fluid layers: the role of bottom friction and fluid layer depth. *Phys. Rev.* E **67**, 066303.

Cuevas, S., Smolentsev, S. & Abdou, M. 2006 On the flow past a magnetic obstacle. *J. Fluid Mech.* **553**, 227–252.

Griebel, M., Dornseifer, T. & Neunhoeffer, T. 1998 *Numerical Simulation in Fluid Dynamics.* SIAM.

Hansen, A. E., Marteau, D. & Tabeling, P. 1998 Two-dimensional turbulence and dispersion in a freely decaying system. *Phys. Rev.* E **58**, 7261–7271.

Lavrent'ev, I. V., Molokov, S. Yu., Sidorenkov, S. I. & Shishko, A. R. 1990 Stokes flow in a rectangular magnetohydrodynamic channel with nonconducting walls within a non-uniform magnetic field at large Hartmann numbers. *Magnetohydrodynamics* **26** (3), 328–338.

Marteau, D., Cardoso, O. & Tabeling, P. 1995 Equilibrium states of two-dimensional turbulence: an experimental study. *Phys. Rev.* E **51**, 5124–5127.

McCaig, M. 1977 *Permanent Magnets in Theory and Practice*. Wiley.

Messadek, K. & Moreau, R. 2002 An experimental investigation of MHD quasi-two-dimensional turbulent shear flows. *J. Fluid Mech.* **456**, 137–159.

Moreau, R. 1990 *Magnetohydrodynamics.* Kluwer.

Paret, J., Marteau, D., Paireau, O. & Tabeling, P. 1997 Are flows electromagnetically forced in stratified layers two-dimensional? *Phys. Fluids* **7** (10), 3102–3104.

Paret, J. & Tabeling, P. 1997 Experimental observation of the two-dimensional inverse energy cascade. *Phys. Rev. Lett.* **79** (21), 4162–4165.

Potherát, A., Sommeria, J. & Moreau, R. 2000 An effective two-dimensional model for MHD flows with transverse magnetic fields. *J. Fluid Mech.* **424**, 75–100.

Rothstein, D., Henry, E. & Gollub, J. P. 1999 Persistent patterns in transient chaotic fluid mixing. *Nature*, **401** 770–772.

Rossi, L., Vassilicos, J. C. & Hardalupas, Y. 2006*a* Electromagnetically controlled multi-scale flows. *J. Fluid Mech.* **558**, 207–242.

Rossi, L., Vassilicos, J. C. & Hardalupas, Y. 2006*b* Multiscale laminar flows with turbulentlike properties. *Phys. Rev. Lett.* **97**, 144501.

Satijn, M. P., Cense, A. W., Verzicco, R., Clercx, H. J. H. & van Heijst, G. J. F. 2001 Three-dimensional structure and decay properties of vortices in shallow fluid layers. *Phys. Fluids* **13**, 1932–1945.

Smolentsev, S. 1997 Averaged model in MHD duct flow calculations. *Magnetohydrodynamics* **33** (1), 42–47.

Sommeria, J. 1986 Experimental study of the two-dimensional inverse energy cascade in a square box. *J. Fluid Mech.* **170**, 139–168.

Sommeria, J. 1988*a* Electrically driven vortices in a strong magnetic field. *J. Fluid Mech.* **189**, 553–569.

Sommeria, J. 1988*b* Experimental characterization of steady two-dimensional vortex couples. *J. Fluid Mech.* **192**, 175–192.

Sommeria, J. & Moreau, R. 1982 Why, how, and when, MHD turbulence becomes two-dimensional. *J. Fluid Mech.* **118**, 507–518.

Tabeling, P. 2002 Two-dimensional turbulence: a physicist approach. *Phys. Rep.* **362**, 1–62.

Voth, G. A., Haller, G. & Gollub, J. P. 2002 Experimental measurements of stretching fields in fluid mixing. *Phys. Rev. Lett.* **88** (15) 254501.

Voth, G. A., Saint, T. C., Dobler, G. & Gollub, J. P. 2003 Mixing rates and symmetry breaking in two-dimensional chaotic flow. *Phys. Fluids* **15** 2560–2566.

Williams, B. S., Marteau, D. & Gollub, J. P. 1997 Mixing of a passive scalar in magnetically forced two-dimensional turbulence. *Phys. Fluids* **9** 2061–2079.

Zavala Sansón, L., van Heijst, G. J. F. & Backx, N. A. 2001 Ekman decay of a dipolar vortex in a rotating fluid. *Phys. Fluids* **13**, 440–451.